

Hydrogen recovery from ammonia purge gas by a membrane separator: A simulation study

Meysam Maarefian¹ | Samaneh Bandehali² | Shabnam Azami³ |
Hamidreza Sanaeepur²  | Abdolreza Moghadassi²

¹ Razi Petrochemical Company, Imam Khomeini Port, Iran

² Department of Chemical Engineering, Faculty of Engineering, Arak University, Arak, Iran

³ Chemical Engineering Department, Islamic Azad University, Farahan Branch, Farmahin, Iran

Correspondence

Hamidreza Sanaeepur, Department of Chemical Engineering, Faculty of Engineering, Arak University, Arak 38156-8-8349, Iran.

Email: h-sanaeepur@araku.ac.ir; h.sanaeepur@yahoo.com

Summary

In this study, a two-dimensional mathematical model is proposed for modeling the hollow fiber membrane (HFM) separators for hydrogen (H₂) recovery unit implemented in the Razi Petrochemical Company (Imam Khomeini Port, Iran) to capture hydrogen from ammonia (NH₃) purge gas. In this regard, computational fluid dynamics is applied to solve the equations of momentum and mass transfer in the laminar flow conditions. Axial and radial diffusion for mass transfer inside the membrane fibers and axial diffusion within the shell side of separator were considered. The distributions of concentration, velocity, and mass transfer fluxes were achieved by the model. As the new insights, the effects of feed flow rate and feed gas concentration on mass transfer of H₂ were investigated. Moreover, fluid velocity profile and H₂ fluxes in the tube (fiber), membrane, and shell sides of the HFM separator were studied. The results of simulation were compared with the industrial data and showed that the present developed model has excellent agreement with the experimental data with a low mean deviation value of 3.5%.

KEYWORDS

hollow fiber separator, membrane, Ammonia purge gas, H₂ separation, membrane, numerical simulation

Nomenclature: C_0 , inlet H₂ concentration in the feed (shell) side, mol/m³; $C_{H_2\text{-membrane}}$, H₂ concentration in the membrane, mol/m³; $C_{H_2\text{-shell}}$, H₂ concentration in the shell, mol/m³; $C_{H_2\text{-tube}}$, H₂ concentration in the tube, mol/m³; C_i , concentration of any species, mol/m³; $D_{H_2\text{-membrane}}$, H₂ diffusion coefficient into the membrane, m²/s; $D_{H_2\text{-shell}}$, H₂ diffusion coefficient into the shell, m²/s; $D_{H_2\text{-tube}}$, H₂ diffusion coefficient in the tube, m²/s; D_{gas} , gas phase diffusion coefficient, m²/s; $D_{i\text{-shell}}$, diffusion coefficient of any species in the shell, m²/s; D_{liquid} , liquid phase diffusion coefficient, m²/s; L , length of the fiber, m; m , partition coefficient; N_i , total flux for all species, mol/m²s; r_1 , inner radius of tube, m; r_2 , outer radius of tube, m; r_3 , inner radius of shell, m; R , overall reaction rate for all species, mol/m³s; \mathfrak{R} , inner radius of module, m; u , average velocity, m/s; V_z , velocity in the module, m/s; $V_{z\text{-shell}}$, velocity in the shell, m/s; $V_{z\text{-tube}}$, velocity in the tube, m/s; z , axial distance, m; p , pressure, Pa; T , temperature, °K; v , fluid velocity, m/s; n , number of fibers, –

Greek symbols: ε , porosity; τ , tortuosity; Φ , module volume fraction, m³; ρ , density, g/l; η , viscosity, cp

Subscripts: Shell, space around the fibers in the HFMC; Tube, inner part of the fiber

Abbreviations: FEM, Finite element method; HFM, hollow fiber membrane; HFMC, hollow fiber membrane contactor; CFD, computational fluid dynamics; H₂, hydrogen; MEA, monoethanolamine; TEA, triethanolamine

1 | INTRODUCTION

Hydrogen (H_2) is the most abundant element in the world.¹ It can be used as an important energy carrier and fuel in the transport systems. However, available pure H_2 is very low. A large amount of available H_2 is in combination with oxygen and carbon. Water, biomass, and hydrocarbons are three different forms of H_2 storing systems.^{2,3} Nowadays, membrane-based technology has been considered as a powerful technique for various separation processes. Membrane-based process units have a compact size, high efficiency, low maintenance, low-energy consumption, low capital investment, ease of operation, and high flexibility.⁴⁻⁷ Hence, membrane technology can be preferred to other separation processes such as adsorption, absorption, and cryogenic distillation. The first H_2 /nitrogen (N_2) membrane separation unit in a large-scale industrial plant was implemented by Monsanto in the ammonia purge gas unit in 1980.^{4,8,9} Other major H_2 separation processes include the separation of H_2 from methane (CH_4) (natural gas refining) and adjusting the carbon monoxide (CO)/ H_2 ratio in the syngas process.^{10,11}

H_2 is a small and noncondensable gas with a high diffusion rate in glassy polymers. The common polymeric membrane materials for H_2 separation are polysulfones, polycarbonates, cellulose acetates, polyamides, polyimides, and fluoropolymers.¹²⁻¹⁵ Among the membrane configurations, hollow fiber membrane (HFM) has the highest surface area in comparison with the other modules such as spiral wound and plate and frame.^{10,16,17}

Gas-liquid HFM contactors (HFMCs) are proposed as favorable equipments, which take the advantages of both the HFMs and gas-liquid contactors. They are preferred due to high surface area, no phase interpenetrations, and the ease of scale-up and down. In addition, they have no operational problems that usually occur in conventional equipment, such as flooding, weeping, loading, entrainment, and foaming. In recent years, many studies have been conducted in modeling and simulation of HFMCs by considering the influence of various parameters such as gas and liquid flow rates, absorbent types, fluid velocities, and pressure.¹⁸⁻²⁸ Membrane modeling can be done for a better material selection, adjusting the operating conditions and design of the membrane modules. Moreover, simulation of HFMs can help to predict optimum operating conditions for minimization of economic costs.^{23,29-37} In addition to process conditions, membrane materials and configurations have also been considered in many studies. For example, HFMCs in nonwetted conditions, which apply hydrophobic membrane materials, showed usually better performances

due to low resistance against the species transport through the membrane pores.³⁸

Aghaeinejad-Meybodi et al.³⁹ have modeled the inorganic silica membranes in cocurrent, countercurrent, and crosscurrent flow conditions in order to optimize the process of H_2 separation from methanol steam reforming products (with CO as a major component). The results showed that by a single-stage silica membrane for H_2 /CO, separation can be obtained high purity of H_2 (99 mol.%, and 0.4 mol.% of CO) at a pressure gradient equal to 3 bar. Peer et al.⁴⁰ have also modeled the H_2 /CO separation (syngas ratio adjustment) with polyimide HFMCs. They concluded that both the plasticization and concentration polarization, which are induced by CO transfer, reduce the H_2 permeance in the mixed gas experiment. Mansourpour et al.⁴¹ through a three-dimensional computational fluid dynamics (CFD) model investigated the steady and unsteady state H_2 / N_2 separation by Pd/ α - Al_2O_3 HFMs. The effects of operating conditions on concentration polarization were also examined by applying flux as the sensitivity factor. They observed a good conformity between the CFD results and the experimental data. Wang et al.⁴² have reported an experimental and modeling study of H_2 / N_2 separation in a thin Pd/ α - Al_2O_3 HFM. In order to determine the membrane parameters, they applied pure gas experimental data. Applying the data, H_2 flux in the mixed gas experiments was simulated, which led to an excellent agreement between the model results and the experimental data.

In addition to the abovementioned studies, many research studies have been devoted to simulation or modeling study of H_2 /CO₂ and H_2 /CH₄ separations.⁴³⁻⁴⁵ But there is rarely a comprehensive mathematical modeling study for investigating the separation performance of HFMs in H_2 recovery from ammonia (NH₃) purge gas. Recently, Ardaneh et al.⁴⁶ reported a 2D mathematical model for H_2 recovery from ammonia purge gas by polyimide HFMs. They investigated different operating conditions and geometrical factors for a two-stage membrane module. The results showed that H_2 recovery reduces by 4.82% through increasing the feed flow rate from 0.3847 to 0.5014 kg/s in the second stage, in comparison with the first stage that H_2 recovery reduces 5.887% at a constant pressure. Moreover, H_2 recovery increased by increasing the fiber lengths. They also showed that the countercurrent flow has a higher performance than the cocurrent one at the same operating conditions.

The present study aims to provide a new 2D mathematical model for HFMs, which is capable to evaluate the influence of different factors on the membrane performance. To give better insight, the model will be validated by the data obtained from an industrially implemented

hydrogen recovery unit (HRU) from ammonia purge gas in Razi Petrochemical Company, Imam Khomeini Port, Iran. The above-mentioned report by Ardaneh et al⁴⁶ has also presented mathematical modeling of HFMs and investigated different flow patterns and geometrical parameters of the polyimide HFMs. In the present research, for the first time, a comprehensive CFD model was presented for an industrial scale, single-stage, polyamide HFM separator unit using the real operating conditions for H₂ recovery from ammonia (NH₃) purge gas. As the new and remarkable insights, the effects of feed gas concentration, fluid velocity and H₂ fluxes in the tube (fiber), membrane, and shell sides of the HFM separator were investigated, which had not been considered in the previous publications.

2 | MODELING

Modeling makes a possibility for investigating the influence of different parameters on the system performances with the least cost. Here, the equations of mass and momentum transfers for an HFM separator are developed.

2.1 | Modeling of mass and momentum transfers in the membrane

Two-dimensional mathematical modeling was applied for an HFM separator, which is used in H₂ recovery from ammonia purge gas. Figure 1 illustrates four identical HFM modules applied for separating H₂ from ammonia purge gas in Razi Petrochemical Company, Imam Khomeini Port, Iran. Also, it represents a schematic for each of the HFM separators, which are applied for modeling. A feed gas mixture enters into the shell with the composition of 77 mol.% H₂, 17.5 mol.% N₂, and 5.5 mol.% CH₄ at 58°C and 88.82 atm. H₂ penetrates through the porous polyamide hollow fibers and leaves the separator as a permeate stream with the purity of 92 mol.%.

2.2 | Assumptions

Some assumptions used this model can be given as follows.

- Steady-state isothermal flow considers without any considerable frictional losses and stresses.
- No chemical reactions occur in the membrane fibers.

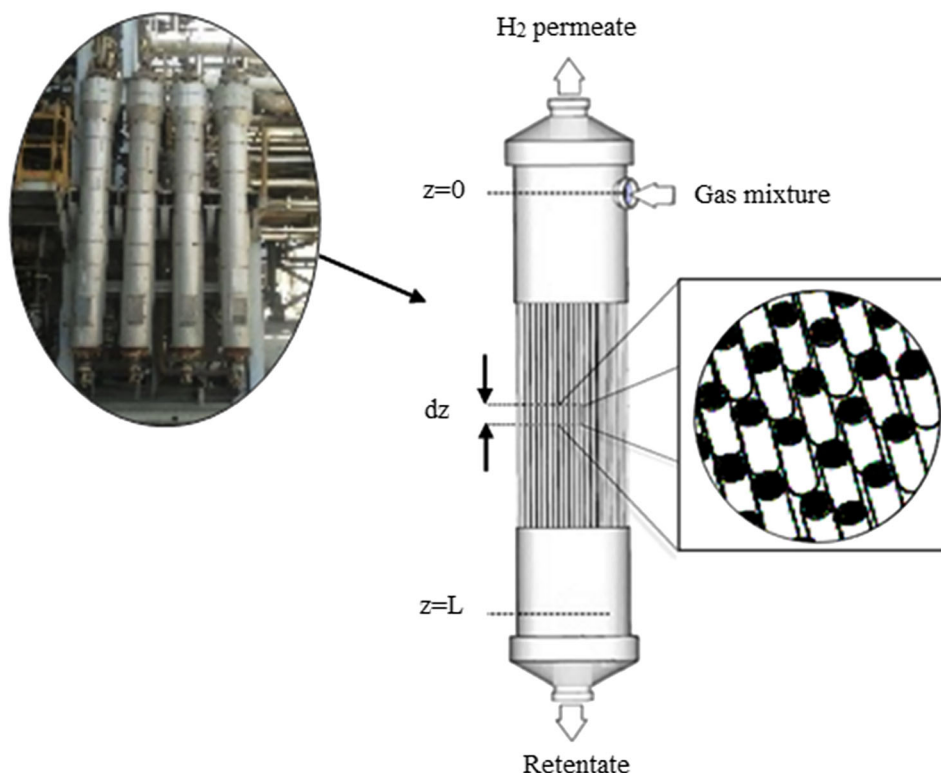


FIGURE 1 Four identical hollow fiber membrane modules and a schematic for one of the membrane modules applied for separating H₂ from ammonia purge gas in Razi Petrochemical Company, Imam Khomeini Port, Iran. The photo of real modules was taken with permission from Razi Petrochemical Company [Colour figure can be viewed at wileyonlinelibrary.com]

- The hollow fibers do not show deformations and leakages for the gas losses.
- The hollow fibers are uniform.
- Concentration polarization can be neglected.
- The membrane module is at adiabatic conditions with no heat transfers between the shell outside, the wall and the atmosphere.

2.3 | Governing equations of the tube side

A general form of the continuity equation governing all the species (i) transports in the HFM separation system is as follows^{47,48}:

$$\frac{\partial C_i}{\partial t} = -(\nabla \cdot C_i V) - (\nabla \cdot J_i) + R_i, \quad (1)$$

where C_i is the i -component concentration, J_i is diffusive flux, and R_i is the rate of reaction for species i . V and t are velocity and time, respectively. Each of the fibers in an HFM separator has a cylinder shape that can be modeled in cylindrical coordinates (radius r , azimuth θ , and elevation z). According to the proposed assumptions in the text, a constant azimuth θ and also a radial symmetry are the majority of presenting a 2D mathematical model. Considering Ficks law of diffusion for mass transport of species, the continuity equation for H_2 transport in the tubes (fibers) in cylindrical coordinate at the steady-state condition is

$$D_{H_2\text{-tube}} \left[\frac{\partial^2 C_{H_2\text{-tube}}}{\partial r^2} + \frac{1}{r} \frac{\partial C_{H_2\text{-tube}}}{\partial r} + \frac{\partial^2 C_{H_2\text{-tube}}}{\partial z^2} \right] = -V_{z\text{-tube}} \frac{\partial C_{H_2\text{-tube}}}{\partial z}. \quad (2)$$

Here, the radial and axial directions in the cylindrical coordinate are shown by r and z , respectively. $D_{H_2\text{-tube}}$, $C_{H_2\text{-tube}}$ and $V_{z\text{-tube}}$, respectively, are known as diffusion coefficient, concentration, and fluid velocity in the tube. Since “ z ” is much larger than “ r ,” for solving the equation in a numerical manner on “ z ,” scaling factor is applied. Laminar fluid flow with constant density and viscosity is considered in a circular porous tube. The incompressible Navier–Stokes equation in cylindrical coordinates is followed by^{49–51}

$$-\nabla \cdot \eta \left(\nabla V_{z\text{-tube}} + (\nabla V_{z\text{-tube}})^T \right) + \rho (V_{z\text{-tube}} \cdot \nabla) V_{z\text{-tube}} + \nabla p = F, \quad \nabla \cdot V_{z\text{-tube}} = 0 \quad (3)$$

where η represents dynamic viscosity of the fluid (kg/m.s), $V_{z\text{-shell}}$ (m/s) denotes velocity, ρ (kg/m³) is the fluid density, p equals pressure (atm), and F represents a body force term (N/m³).

The boundary conditions for tubes are defined as follows:

Continuity equation:

$$C_{H_2\text{-tube}} = 0 \quad @ \quad z = 0 \quad \text{Concentration} \quad (4)$$

$$n \cdot (-D \nabla C_{H_2\text{-tube}}) = 0, \quad @ \quad z = L \quad \text{Convective flux} \quad (5)$$

where C_{H_2} (mol/m³) represents for H_2 concentration inside the tube. It is assumed that the boundary condition (convective flux) is constant in all fibers. According to this assumption, the diffusion flux is zero across the tubes.

$$\frac{\partial C_{H_2\text{-tube}}}{\partial r} = 0 \quad @ \quad r = 0 \quad (\text{symmetry}) \quad (6)$$

$$C_{H_2\text{-tube}} = C_{H_2\text{-membrane}} \times m \quad @ \quad r = r_1 \quad (7)$$

Here $C_{H_2\text{-membrane}}$ (mol/m³) is H_2 concentration in the membrane and m is a partition coefficient, which depends on the equilibrium solute concentrations two sides of a boundary and is obtained from the concentration ratio of liquid to gas at the equilibrium.⁵²

Momentum equation:

$$\frac{\partial V_{z\text{-tube}}}{\partial r} = 0 \quad @ \quad r = 0 \quad \text{Symmetry boundary} \quad (8)$$

$$V_{z\text{-tube}} = 0 \quad @ \quad r = r_1 \quad \text{Wall, no slip velocity} \quad (9)$$

$$V_{z\text{-tube}} = V_0 \quad @ \quad z = 0 \quad \text{Inlet velocity} \quad (10)$$

$$p = p_0 \quad @ \quad z = L \quad \text{Outlet boundary} \quad (11)$$

$C_{H_2\text{-tube}}$ (mol/m³), p_0 (Pa), and V_0 (m/s) are H_2 concentration, output pressure, and input velocity in the tube, respectively. Indeed, at the fluid-porous medium interface, the slip velocity is usually considered. However, the slip velocity in hollow fibers can be neglected due to the low permeability in open pores. It results from the fact that the aspect ratio between the pore diameter and the height of the fiber is small. Therefore, it is considered that there is no slip velocity at the fluid-porous medium interface.⁵³

2.4 | Membrane equations

The continuity equation in the steady-state condition for H_2 transfer within the membrane is only defined by diffusion. This equation is written as.

$$D_{H_2-membrane} \left[\frac{\partial^2 C_{H_2-membrane}}{\partial r^2} + \frac{1}{r} \frac{\partial C_{H_2-membrane}}{\partial r} + \frac{\partial^2 C_{H_2-membrane}}{\partial z^2} \right] = 0 \quad (12)$$

In this equation, $C_{H_2-membrane}$ (mol/m³) and $D_{H_2-membrane}$ (m²/s) are H₂ concentration and its diffusion coefficient in the membrane, respectively. The reaction rate is not considered because of the absence of chemical reactions into the membranes. Mass transfer is performed only via molecular diffusion, and there is no bulk diffusion. Therefore, Ficks law of diffusion can be applied alone in the membranes.

The boundary conditions in the membranes are.

$$-D_{H_2} \nabla C_{H_2-membrane} = 0 \quad @ \quad z = 0 \text{ and } z = L \quad (13)$$

$$C_{H_2-membrane} = \frac{C_{H_2-tube}}{m} \quad @ \quad r = r_1 \quad (14)$$

$$C_{H_2-membrane} = C_{H_2-shell} \quad @ \quad r = r_2 \quad (15)$$

2.5 | The governing equations in the shell

Based on the Ficks law of diffusion, the continuity equation in the steady-state condition for H₂ transfer in the shell side of HFM separator at cylindrical coordinate can be written as.

$$D_{H_2-shell} \left[\frac{\partial^2 C_{H_2-shell}}{\partial r^2} + \frac{1}{r} \frac{\partial C_{H_2-shell}}{\partial r} + \frac{\partial^2 C_{H_2-shell}}{\partial z^2} \right] = -V_{z-shell} \frac{\partial C_{H_2-shell}}{\partial z} \quad (16)$$

By assuming uniform velocity on the shell side, the Navier–Stokes motion equation is applied in this area. In this case, considering the constant fluid density and viscosity, Navier–Stokes equation is defined as follows⁴⁸:

$$-\nabla \cdot \eta \left(\nabla V_{z-shell} + (\nabla V_{z-shell})^T \right) + \rho (V_{z-shell} \cdot \nabla) V_{z-shell} + \nabla p = F$$

$$\nabla \cdot V_{z-shell} = 0 \quad (17)$$

where $V_{z-shell}$ (m/s) is velocity vector, η is dynamic viscosity of the fluid (kg/m.s), and ρ (kg/m³) is the fluid density. p indicates the pressure (atm), and F represents a body force term (N/m³). Happel model can be applied for estimating the free surface radius (r_3) in the shell⁵⁴:

$$r_3 = \left(\frac{1}{1-\phi} \right)^{1/2} r_2 \quad (18)$$

where r_2 and ϕ are the outer radius of the membrane (tube) and volume fraction of the fibers in the shell, respectively. It should be notified that the present study is focused on the entire HFM module, and the adoption of Happels free surface model enables the simulation to be simplified into the one of single fiber and its local shell space. Happels model is used for free surfaces. It considers a cylindrical arrangement and investigates the flow of fluid in a unit cell. In this model, a fiber is located as an inner cylinder and the fluid is considered on the surface of the fiber or as an outer cylinder. Happels model considers that all fibers have the same contribution in the separation process. Moreover, no-slip boundary conditions are assumed on the fiber surfaces. This model simplifies the calculation of effective properties.⁵³

The volume fraction of the fibers (ϕ) is calculated by the below equation:

$$1 - \phi = \frac{nr^2}{\mathfrak{R}^2} \quad (19)$$

where n is the number of fibers and \mathfrak{R} is the modules inner radius.

The velocity of fluid in the shell side of HFM separator can be determined by Happels free surface model.^{54,55} However, Navier–Stokes equation is more usual and frequently used for calculation of the fluid velocity in the shell for all membrane geometries.⁴⁸ The boundary conditions of the shell are written as.

Continuity equation:

$$C_{H_2-shell} = C_{H_2-membrane} \quad @ \quad r = r_2 \text{ Concentration} \quad (20)$$

$$C_{H_2-shell} = C_{H_2} \quad @ \quad r = r_3 \text{ Concentration} \quad (21)$$

$$C_{H_2-shell} = C_{H_2} \quad @ \quad z = 0 \text{ Concentration} \quad (22)$$

$$n \cdot (-D_{H_2-membrane} \nabla C_{H_2-membrane}) = 0 \quad @ \quad z = L \text{ Convective flux} \quad (23)$$

Momentum equation:

$$V_z = 0 \quad @ \quad r = r_2 \text{ Wall, no-slip} \quad (24)$$

$$V_z = V_{z,0} \quad @ \quad r = r_3 \text{ Open boundary} \quad (25)$$

$$V_z = V_{z,0} \quad @ \quad z = 0 \text{ Inlet} \quad (26)$$

$$p = p_0 \quad @ \quad z = L \text{ Outlet} \quad (27)$$

$C_{H_2-shell}$ (mol/m³), p_0 (Pa), and $V_{z,0}$ (m/s) are H₂ concentration, output pressure, and input velocity in the shell, respectively.

2.6 | Procedure of numerical solution

The equations of the proposed model can be solved by considering the proper boundary conditions according to the industrial membrane separators implemented in the HRU in order to H_2 capture from NH_3 purge gas in Razi Petrochemical Company, Imam Khomeini Port, Iran. The applied physical characteristics in the model are represented in Table 1. Numerical solution is conducted by Comsol Multiphysics version 4.2 that applies the finite element method. The UMFPACK solver is also applied, which is an operational and accurate solver for the cases with symmetrical geometry. The capability, power, and accuracy of this method for membrane processes have been proven by some authors.^{26,56-60}

Figure 2 shows a representation for a three-sectional domain, which is considered in this paper. COMSOL provides an isotropic triangular mesh in this case. A reducing scale factor considers due to the larger length of the membrane fibers in comparison with their radius. Adaptive mesh tool in COMSOL was applied to optimize the mesh numbers in the model domain, ie, the mesh independency test. Thoroughly, the number of meshes reached 1875, by using a scale factor of

TABLE 1 The applied parameters in the present model

Parameter	Value
$D_{\text{shell}}, \text{cm}^2/\text{s}$	8.778×10^{-4}
$D_{\text{tube}}, \text{cm}^2/\text{s}$	2.3038×10^{-3}
ε	0.78
$D_{\text{membrane}}, \text{cm}^2/\text{s}$	6.87×10^{-7}
r_1, m	5×10^{-5}
r_2, m	9×10^{-5}
r_3, m	1.5×10^{-4}
\mathcal{R}, m	0.065
L, m	2.935
n	76 000
$Q_s, \text{m}^3/\text{s}$	2.537×10^{-4}
$C_0, \text{mol}/\text{m}^3$	0.5
p_0, atm	88.82
$\rho, \text{g}/\text{cm}^3$	0.4143
$\eta, \text{kg}/\text{m.s}$	1.0×10^{-6}
Scale	4000

Note. It should be notified that the measurable parameters were taken with permission from the real hollow fiber membrane modules in Razi Petrochemical Company, Imam Khomeini Port, Iran. The other parameters were determined by the methods and formula that come in the text.

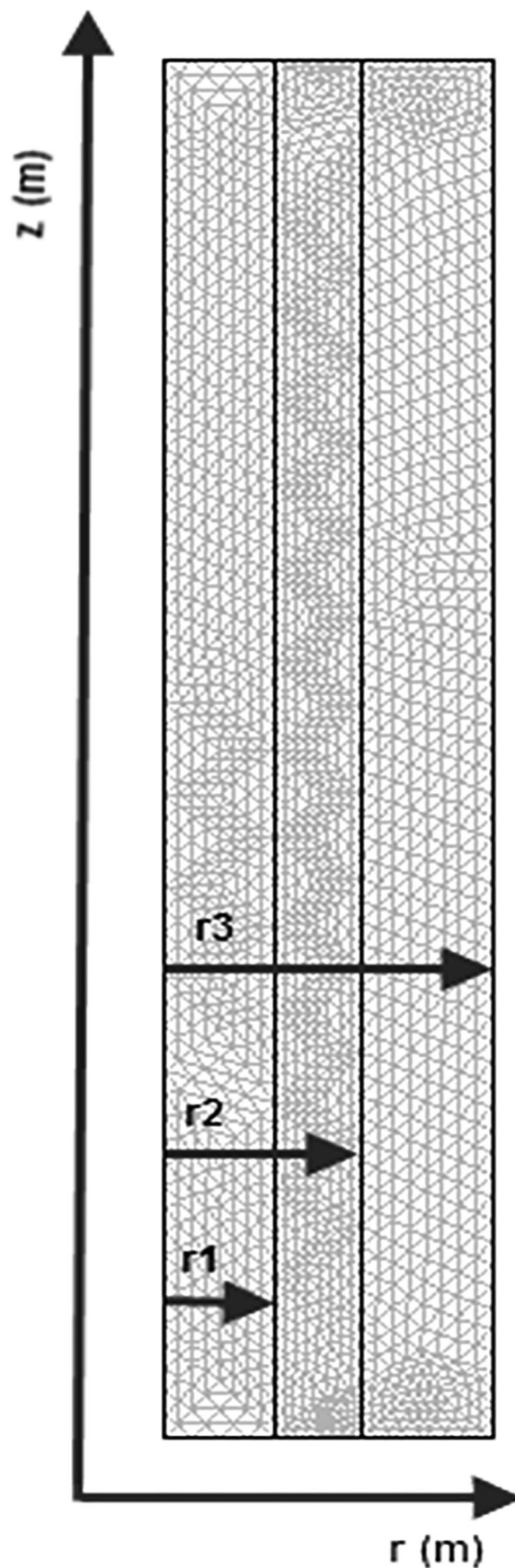


FIGURE 2 The three-sectional model domain and the generated meshes for numerical solution of the model equations

4000 for z coordinate. It is noteworthy to mention that the interfaces between neighbor domains have finer meshes in order to enhance the precision of the model solution.

The porosity of hollow fibers, ε , is determined by Equation (28)^{61,62}:

$$\varepsilon(\%) = \frac{(W_{\text{wet}} - W_{\text{dry}})}{\rho_f V} \times 100, \quad (28)$$

where W_{wet} and W_{dry} are the wet and dry weights of a hollow fiber (g), ρ_f is the wetting liquid (isopropanol) density (g/cm^3), and V (cm^3) is the volume of the hollow fiber. The experimental data of porosity were measured for 3 times, and the mean value of these measurements was reported as the membrane porosity.

3 | RESULTS AND DISCUSSION

3.1 | H_2 concentration profile in the HFM separator

Figure 3 represents the H_2 concentration profile in all the model domains, ie, tube (fiber), membrane, and shell sides of the HFM separator. On the shell (right-hand side of the figure), the purge gas stream has its maximum H_2 concentration ($0.5 \text{ mol}/\text{m}^3$) at $z = 0$. H_2 passes across the membrane and transports from the shell into the fiber (left-hand side of the figure) due to the H_2 concentration difference in two membrane sides. There is only a radial flux in the membrane with the diffusion mechanism, while the flux is generally in the axial direction for the shell and fiber. The maximum H_2 concentration obtains at the fiber output ($z = L$).

FIGURE 3 H_2 concentration distribution in the hollow fiber membrane separator; $r_1 = 5 \times 10^{-5} \text{ m}$, $r_2 = 9 \times 10^{-5} \text{ m}$, $r_3 = 1.5 \times 10^{-4} \text{ m}$, $L = 2.935 \text{ m}$, $D_{\text{shell}} = 8.778 \times 10^{-4} \text{ cm}^2/\text{s}$, $m = 0.82$, $Q_{\text{shell}} = 2.537 \times 10^{-4} \text{ m}^3/\text{s}$, and $C_0 = 0.5 \text{ mol}/\text{m}^3$. A three-dimensional view is only presented for better understanding the results [Colour figure can be viewed at wileyonlinelibrary.com]

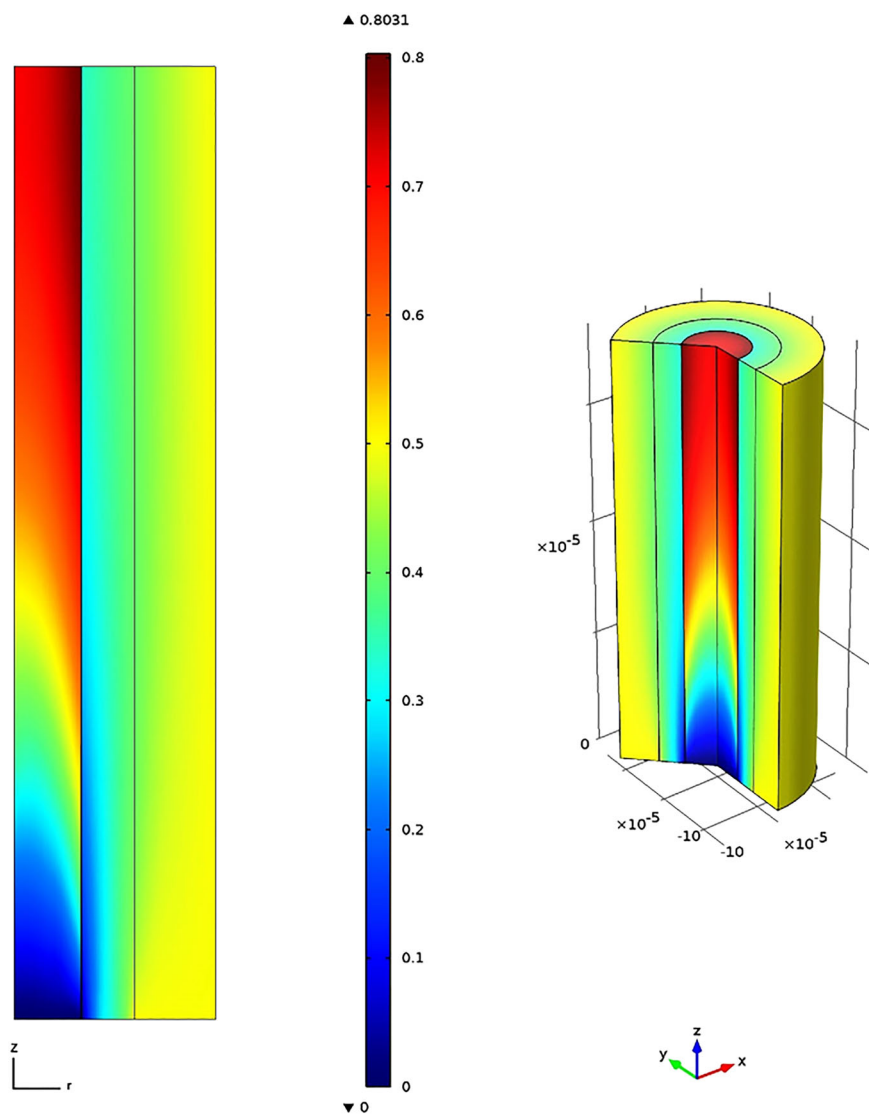


Figure 4 shows the total H_2 concentrations in the radial direction and at different positions ($z = 0$, $z = L/3$, $z = L/2$, and $z = L$) of the HFM separator. As seen, from r_3 to r_2 (in the shell side), the H_2 concentration decreases or the concentration gradient increases. This is a common behavior for mass transfer towards the membrane. From r_2 to r_1 , in a short distance (or across the membrane), H_2 concentration increases very sharply due to a large difference in H_2 concentration gradients in the tube (fiber) and shell sides. From r_1 to the center of a fiber ($r = 0$), H_2 is significantly concentrated as compared with its concentration in the shell. The H_2 concentration value is also increased from $z = 0$ to $z = L$ at axial direction of the separator that was previously discussed. The contact area or the membranes effective surface area directly affects the separation performance of HFM separator.

3.2 | Velocity in the shell side

Navier-Stokes equation was applied to obtain the fluid velocity in the shell side of the HFM separator. Figure 5 shows the z -velocity as a function of radius (from $r_2 = 9 \times 10^{-5}$ m to $r_3 = 1.4 \times 10^{-4}$ m) in four selected cross sections of $z = 0$, $L/3$, $L/2$, and L in the shell side. If there was not a continuous fluid permeation into the membrane, a parabolic velocity profile would be attained. Here, the velocity increases with increasing the permeation into the membrane because the gas molecules attain a higher space with a lower

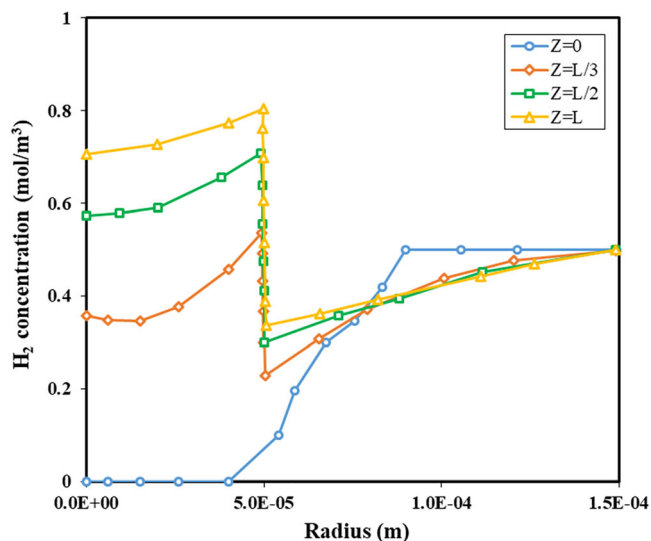


FIGURE 4 H_2 concentration in the tube, membrane, and shell sides of the hollow fiber membrane separator at radial direction with $C_0 = 0.5$ mol/m³ and $Q_{\text{shell}} = 2.537 \times 10^{-4}$ m³/s [Colour figure can be viewed at [wileyonlinelibrary.com](#)]

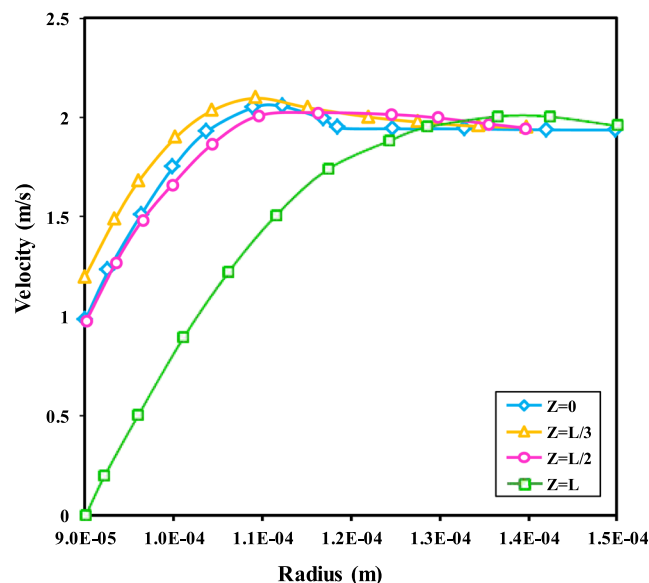


FIGURE 5 The z -velocity profile in the shell side of the hollow fiber membrane separator at different radii with $C_0 = 0.5$ mol/m³ and $Q_{\text{shell}} = 2.537 \times 10^{-4}$ m³/s [Colour figure can be viewed at [wileyonlinelibrary.com](#)]

collision for their motion. Moreover, an increase in the H_2 mass transfer from the shell into the fibers leads to the more uniform distribution of H_2 velocity in the shell side. Figure 5 shows that for all the curves, it happens lower velocities at lower radii and then the velocity increases in a short distance from the membrane wall. For $z = L$, velocity reaches zero near the membrane wall because of the viscosity effects or no-slip condition. Next, the velocity reaches a plateau with a constant value about 2 m/s at the radius of 1.3×10^{-4} m (close to the $r_3 = 1.4 \times 10^{-4}$ m). The results also show that with the increment in z values, the velocity tends to plateau at higher radii. This means less potential for convection mass transfer and reducing from the removal efficiency.

Figure 6 shows the velocity changes in the shell side as a function of input feed flow rate in different radii (from $r_2 = 9 \times 10^{-5}$ to $r_3 = 1.4 \times 10^{-4}$ m) at a constant length ($z = L$). As shown, the velocity increases with increasing the input feed flow rate. Moreover, it reaches to its maximum value or to a plateau at lower radii. Therefore, it can be concluded that the alteration of velocity is remarkably related to input feed flow rate. It can also be observed that the initial slope of the curves increases with the increase in flow rate. This means higher velocities near the fibers and hence higher mass transfer rates. Moreover, when the input flow rate increases in the HFM separator, the residence time of the molecules decreases that leads to a higher productivity.

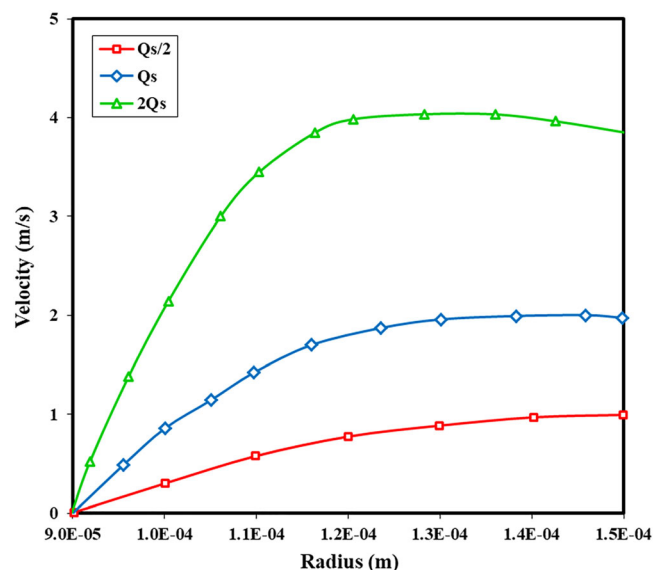


FIGURE 6 The effect of feed flow rate on the shell side velocity of hollow fiber membrane separator at different radii in a constant length ($z = L$) with $C_0 = 0.5 \text{ mol/m}^3$ and $Q_s = Q_{\text{shell}} = 2.537 \times 10^{-4} \text{ m}^3/\text{s}$ [Colour figure can be viewed at wileyonlinelibrary.com]

3.3 | Concentration of H_2 in the tube side

Knowing how the concentration distribution of penetrant gases is in the membrane fibers is of great importance for design and optimization of the separation process. Figure 7 shows H_2 concentration profile in the hollow

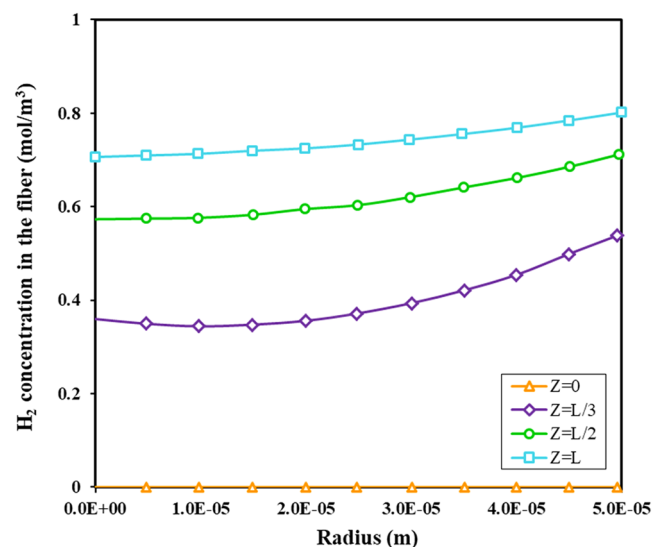


FIGURE 7 H_2 concentration in the tube side of hollow fiber membrane separator at different fiber radii for different axial positions ($z = 0$, $z = L/3$, $z = L/2$, and $z = L$) with $C_0 = 0.5 \text{ mol/m}^3$ and $Q_{\text{shell}} = 2.537 \times 10^{-4} \text{ m}^3/\text{s}$ [Colour figure can be viewed at wileyonlinelibrary.com]

fibers of HFM separator in the case of fiber radius. The curves were produced in constant feed concentration and flow rate at different (scaled) axial positions ($z = 0$, $z = L/3$, $z = L/2$, and $z = L$). Generally, H_2 concentration increases by increasing the fiber radius. H_2 concentration changes with a mild slope near the fiber center ($r = 0$) and then it rises with a steep slope up to $r = r_1$ (the membrane interface). Moreover, it increases by the increment in the axial direction from $z = 0$ to $z = L$. The lowest H_2 concentration is observed for $z = 0$, at the fiber inlet, and the highest for $z = L$, at the fiber outlet. Since the mass transfer is directly proportional to H_2 concentration gradient, it can be expected the more mass transfers with lower fiber radii and higher lengths.

3.4 | H_2 mass transfer flux

The distributions of convective and diffusive mass transfer fluxes for H_2 transfer in fiber (tube) side of the membrane in the radial direction at different positions ($z = 0$, $z = L/3$, $z = L/2$, and $z = L$) are shown respectively in Figures 8A and 8B. In Figure 8A, the convective flux is zero at the fiber inlet ($z = 0$). The convective flux increases from the fiber center ($r = 0$) to the gas-membrane interface ($r = r_1$, the internal wall of the fiber) due to the increase in mass transfer driving force. Moreover, the velocity changes have a significant effect on the convective flux. On the other hand, as seen in Figure 8B, in the lower part of the fiber ($z = 0$), diffusive flux is greater than the convective flux (Figure 8A). Afterwards, in the major parts of the membrane length in Figures 8A and 8B, the convective flux increases as it will be greater than diffusive flux in the axial direction of the fibers because of greater velocities in the axial direction.

3.5 | The effect of initial feed concentration

Figure 9 shows the effect of initial feed concentration (in the shell) on the H_2 concentration distribution in the tube. As shown, by increasing the feed concentration, H_2 concentration in the tube increases. The reason is an increase in driving force (H_2 concentration gradient) by the increase in feed concentration. The effect of feed concentration is more around the gas-membrane interface ($r = r_1$) due to the more mass transfer rates in this region. Near the center of the fibers ($r = 0$), H_2 concentration decreases sharply due to the governing of convection in this case.

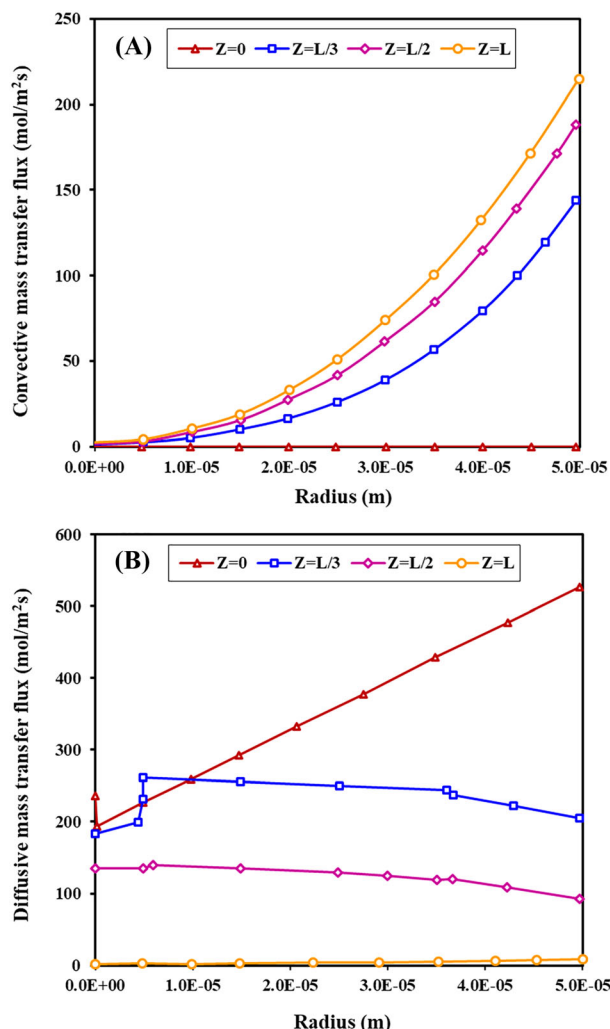


FIGURE 8 The distributions of (A) convective and (B) diffusive mass transfer fluxes of H₂ in radial direction at tube side of the membranes in the hollow fiber membrane separator with $C_0 = 0.5 \text{ mol/m}^3$ and $Q_{\text{shell}} = 2.537 \times 10^{-4} \text{ m}^3/\text{s}$ [Colour figure can be viewed at [wileyonlinelibrary.com](#)]

3.6 | Model validation

A series of actual industrial data from the HFM separators implemented in HRU in order to capture the H₂ from NH₃ purge gas in Razi Petrochemical Company, Imam Khomeini Port, Iran, are used to validate the model results. Sampling was carried out via two sampling valves, which are located at input and output of the HFM separator (Table 2). Variations in the H₂ concentration in the feed (input) are because of H₂ concentration, which is delivered to the plant as well as the operating conditions at different 4 months of operation. Gas chromatography (GC) was used to analyze the gas samples from the separator with an Agilent instrument (Agilent Technologies, Model 6890 N, Network GC System, Netherlands) equipped with a thermal conductivity detector. A stream of argon was applied as a carrier gas. Five

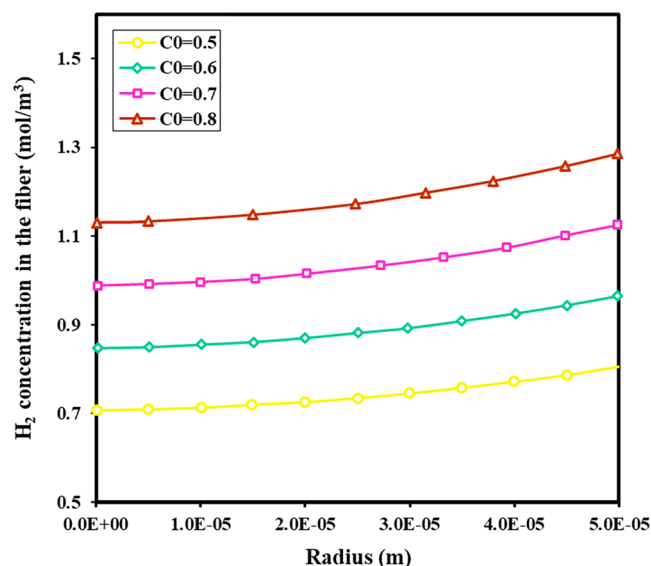


FIGURE 9 The effect of feed concentration on the H₂ concentration in the tube side of the hollow fiber membrane separator with $Q_{\text{shell}} = 2.537 \times 10^{-4} \text{ m}^3/\text{s}$ in a constant length ($z = L$) [Colour figure can be viewed at [wileyonlinelibrary.com](#)]

TABLE 2 Comparison between the model results and the industrial data with $Q_{\text{shell}} = 2.537 \times 10^{-4} \text{ m}^3/\text{s}$ and z -scale factor = 4000

C _{H2} at Input, mol/m ³	C _{H2} at Output, mol/m ³		
	Experimental	Theoretical	Error, %
0.5	0.74	0.72	2.70
0.57	0.84	0.81	3.57
0.61	0.89	0.86	3.37
0.65	0.95	0.91	4.21
Average			3.5

measurements were done for each sample, and the average value of the measurements was reported with an accuracy of $\pm 1 \text{ mol.}\%$ in H₂ concentration. As seen in Table 2, the model results have good agreement with the experimental data. Mean deviation of the model from the experimental data is determined by the following equation:

$$\text{Error}(\%) = \frac{100}{N} \sum \left| \frac{C_{\text{experimental}} - C_{\text{theoretical}}}{C_{\text{experimental}}} \right|. \quad (29)$$

A mean deviation of 3.5% was obtained by the model that shows a reliable and accurate model. It can be attributed to operating conditions, alteration in feed flow rate and its purity.

4 | CONCLUSIONS

This work presented a two-dimensional CFD model for HFM separators applied for hydrogen (H_2) recovery from ammonia (NH_3) purge gas. The distribution of concentration, the mass transfer flux, and the velocity profile were achieved by the model. The results show that H_2 velocity increases with the increase in gas permeation from the shell to the tube of the separator, and also, it increases with increasing the feed flow rate. Moreover, H_2 is concentrated in the tube side of the HFM separator and its concentration increases with increasing the initial (inlet) H_2 concentration. Also, the convective flux is more than diffusive flux in the radial direction of the tube from the gas-membrane interface ($r = r_1$) to fiber center ($r = 0$) because of the higher velocities far from the membrane walls. Generally, the simulation results were comparable with the experimental data obtained from an industrially implemented HFM separator in HRU from ammonia purge gas, with a low mean error of 3.5%. Therefore, it can be expected that the model will be useful to design and development of HFM separators in H_2 recovery units. However, as a future direction, it can be experienced the model capability with other membrane materials and different geometries.

ORCID

Hamidreza Sanaeepur  <https://orcid.org/0000-0003-3255-9696>

REFERENCES

- Chein R-Y, Chen Y-C, Chang C-S, Chung J. Numerical modeling of hydrogen production from ammonia decomposition for fuel cell applications. *Int J Hydrogen Energy*. 2010;35(2): 589-597.
- Koroneos C, Dompros A, Roumbas G, Moussiopoulos N. Life cycle assessment of hydrogen fuel production processes. *Int J Hydrogen Energy*. 2004;29(14):1443-1450.
- Liu PK, Sahimi M, Tsotsis TT. Process intensification in hydrogen production from coal and biomass via the use of membrane-based reactive separations. *Curr Opin Chem Eng*. 2012;1(3):342-351.
- Ebadi Amooghin A, Sanaeepur H, Moghadassi A, Kargari A, Ghanbari D, Sheikhi Mehrabadi Z. Modification of ABS membrane by PEG for capturing carbon dioxide from CO_2/N_2 streams. *Sep Sci Technol*. 2010;45(10):1385-1394.
- Sanaeepur H, Ebadi Amooghin A, Moghadassi A, Kargari A. Preparation and characterization of acrylonitrile-butadiene-styrene/poly (vinyl acetate) membrane for CO_2 removal. *Sep Purif Technol*. 2011;80(3):499-508.
- Kargari A, Sanaeepur H. Application of membrane gas separation processes in petroleum industry. In: Pant KK, Sinha S, Bajpai S, eds. *Advances in Petroleum Engineering I Refining*. Houston, USA: Studium Press LLC; 2015:592-622.
- Bandehali S, Kargari A, Moghadassi A, Sanaeepur H, Ghanbari D. Acrylonitrile-butadiene-styrene/poly (vinyl acetate)/nanosilica mixed matrix membrane for He/CH_4 separation. *Asia Pac J Chem Eng*. 2014;9(5):638-644.
- Baker RW. *Membrane technology and applications*. 3th ed. West Sussex, UK: John Wiley and Sons Ltd; 2012.
- Sanaeepur H, Kargari A, Nasernejad B, Ebadi Amooghin A, Omidkhah M. A novel Co^{2+} exchanged zeolite Y/cellulose acetate mixed matrix membrane for CO_2/N_2 separation. *J Taiwan Inst Chem Eng*. 2016;60:403-413.
- Baker RW. Future directions of membrane gas separation technology. *Ind Eng Chem Res*. 2002;41(6):1393-1411.
- Catalano J, Baschetti MG, Sarti GC. Influence of the gas phase resistance on hydrogen flux through thin palladium-silver membranes. *J Membr Sci*. 2009;339(1-2):57-67.
- Sanaeepur H, Ebadi Amooghin A, Bandehali S, Moghadassi A, Matsuura T, Van der Bruggen B. Polyimides in membrane gas separation: Monomer's molecular design and structural engineering. *Prog Polym Sci*. 2019;91:80-125.
- Ebadi Amooghin A, Mashhadikhan S, Sanaeepur H, Moghadassi A, Matsuura T, Ramakrishna S. Substantial breakthroughs on function-led design of advanced materials used in mixed matrix membranes (MMMs): A new horizon for efficient CO_2 separation. *Prog Mater Sci*. 2019;102:222-295.
- Sanaeepur H, Ebadi Amooghin A, Bandehali S. *Theoretical gas permeation models for mixed matrix membranes*. Beau Bassin, Mauritius: LAP LAMBERT Academic Publishing; 2018.
- Ebadi Amooghin A, Sanaeepur H, Omidkhah M, Kargari A. "Ship-in-a-bottle," a new synthesis strategy for preparing novel hybrid host-guest nanocomposites for highly selective membrane gas separation. *J Mater Chem A*. 2018;6:1751-1771.
- Xu L, Zhang C, Rungta M, Qiu W, Liu J, Koros WJ. Formation of defect-free 6FDA-DAM asymmetric hollow fiber membranes for gas separations. *J Membr Sci*. 2014;459:223-232.
- Schrotter J-C, Bozkaya-Schrotter B. Current and emerging membrane processes for water treatment. In: Peinemann K-V, Nunes SP, eds. *Membrane Technology, Vol. 4: Membranes for water treatment*. New York: John Wiley & Sons Ltd; 2010:53-88.
- Zhuang L, Guo H, Dai G, Xu Z-I. Effect of the inlet manifold on the performance of a hollow fiber membrane module-A CFD study. *J Membr Sci*. 2017;526:73-93.
- Razavi SMR, Rezakazemi M, Albadarin AB, Shirazian S. Simulation of absorption of CO_2 by solution of ammonium ionic liquid in hollow-fiber contactors. *Chem Eng Process Process Intensif*. 2016;10:27-34.
- Hosseinzadeh A, Hosseinzadeh M, Vatani A, Mohammadi T. Mathematical modeling for the simultaneous absorption of CO_2 and SO_2 using MEA in hollow fiber membrane contactors. *Chem Eng Process Process Intensif*. 2017;111:35-45.
- Darestani M, Haigh V, Couperthwaite SJ, Millar GJ, Nghiem LD. Hollow fibre membrane contactors for ammonia recovery: current status and future developments. *J Environ Chem Eng*. 2017;5(2):1349-1359.
- Boributh S, Assabumrungrat S, Laosiripojana N, Jiratananon R. A modeling study on the effects of membrane characteristics

- and operating parameters on physical absorption of CO₂ by hollow fiber membrane contactor. *J Membr Sci.* 2011;380(1–2):21–33.
23. Saidi M. Kinetic study and process model development of CO₂ absorption using hollow fiber membrane contactor with promoted hot potassium carbonate. *J Environ Chem Eng.* 2017;5(5):4415–4430.
 24. Tantikhajongosol P, Laosiripojana N, Jiraratananon R, Assabumrungrat S. Analytical study of membrane wetting at high operating pressure for physical absorption of CO₂ using hollow fiber membrane contactors. *Chem Eng Res Des.* 2017;126:265–277.
 25. Li Y, Jin P, Song X, Zhan X. Removal of carbon dioxide from pressurized landfill gas by physical absorbents using a hollow fiber membrane contactor. *Chem Eng Process Process Intensif.* 2017;121:149–161.
 26. Maarefian M, Miri T, Sanaeepur H, Rooeentan H, Azami S. CFD simulation of a membrane bioreactor for high saline refinery wastewater treatment. *Desalin Water Treat.* 2017;81:33–39.
 27. Saidi M. Mathematical modeling of CO₂ absorption into novel reactive DEAB solution in hollow fiber membrane contactors: kinetic and mass transfer investigation. *J Membr Sci.* 2017;524:186–196.
 28. Zaidiza DA, Belaissaoui B, Rode S, Favre E. Intensification potential of hollow fiber membrane contactors for CO₂ chemical absorption and stripping using monoethanolamine solutions. *Sep Purif Technol.* 2017;188:38–51.
 29. Choi W, Ingole PG, Park J-S, Lee D-W, Kim J-H, Lee H-K. H₂/CO mixture gas separation using composite hollow fiber membranes prepared by interfacial polymerization method. *Chem Eng Res Des.* 2015;102:297–306.
 30. Khalilpour R, Abbas A, Lai Z, Pinnau I. Analysis of hollow fibre membrane systems for multicomponent gas separation. *Chem Eng Res Des.* 2013;91(2):332–347.
 31. Eslami S, Mousavi SM, Danesh S, Banazadeh H. Modeling and simulation of CO₂ removal from power plant flue gas by PG solution in a hollow fiber membrane contactor. *Adv Eng Softw.* 2011;42(8):612–620.
 32. Sanaeepur H, Hosseinkhani O, Kargari A, Ebadi Amooghin A, Raisi A. Mathematical modeling of a time-dependent extractive membrane bioreactor for denitrification of drinking water. *Desalination.* 2012;289:58–65.
 33. Tantikhajongosol P, Laosiripojana N, Jiraratananon R, Assabumrungrat S. Physical absorption of CO₂ and H₂S from synthetic biogas at elevated pressures using hollow fiber membrane contactors: The effects of Henry's constants and gas diffusivities. *Int J Heat Mass Transf.* 2019;128:1136–1148.
 34. Ansari pour M, Haghshenasfard M, Moheb A. Experimental and numerical investigation of CO₂ absorption using nanofluids in a hollow-fiber membrane contactor. *Chem Eng Technol.* 2018;41(2):367–378.
 35. Cao F, Gao H, Li H, Liang Z. Experimental and theoretical studies on mass transfer performance for CO₂ absorption into aqueous N,N-dimethylethanolamine solution in the polytetrafluoroethylene hollow-fiber membrane contactor. *Ind Eng Chem Res.* 2018;57:16862–16874.
 36. Hajilary N, Rezakazemi M. CFD modeling of CO₂ capture by water-based nanofluids using hollow fiber membrane contactor. *Int J Greenhouse Gas Control.* 2018;77:88–95.
 37. Nakhjiri AT, Heydarinasab A, Bakhtiari O, Mohammadi T. Experimental investigation and mathematical modeling of CO₂ sequestration from CO₂/CH₄ gaseous mixture using MEA and TEA aqueous absorbents through polypropylene hollow fiber membrane contactor. *J Membr Sci.* 2018;565:1–13.
 38. Azari A, Abbasi MA, Sanaeepur H. CFD study of CO₂ separation in an HFMC: Under non-wetted and partially-wetted conditions. *Int J Greenhouse Gas Control.* 2016;49:81–93.
 39. Aghaeinejad-Meybodi A, Ghasemzadeh K, Babaluo AA, Morrone P, Basile A. Modeling study of silica membrane performance for hydrogen separation. *Asia Pac J Chem Eng.* 2015;10(5):781–790.
 40. Peer M, Mehdi Kamali S, Mahdeyarfar M, Mohammadi T. Separation of hydrogen from carbon monoxide using a hollow fiber polyimide membrane: experimental and simulation. *Chem Eng Technol.* 2007;30(10):1418–1425.
 41. Mansourpour Z, Sharafpoor A, Ghaee A. Numerical Study on Concentration Polarization for H₂-N₂ Separation through a Thin Pd Membrane by Using Computational Fluid Dynamics. *Chem Prod Process Model.* 2016;11:89–95.
 42. Wang W, Thomas S, Zhang X, Pan X, Yang W, Xiong G. H₂/N₂ gaseous mixture separation in dense Pd/ α -Al₂O₃ hollow fiber membranes: experimental and simulation studies. *Sep Purif Technol.* 2006;52(1):177–185.
 43. Zhang L, Hu Z, Jiang J. Metal-organic framework/polymer mixed-matrix membranes for H₂/CO₂ separation: a fully atomistic simulation study. *J Phys Chem C.* 2012;116:19268–19277.
 44. Yilmaz G, Keskin S. Predicting the performance of zeolite imidazolate framework/polymer mixed matrix membranes for CO₂, CH₄, and H₂ separations using molecular simulations. *Ind Eng Chem Res.* 2012;51(43):14218–14228.
 45. Búcsú D, Nemestóthy N, Pientka Z, Gubicza L, Bélafi-Bakó K. Modelling of biohydrogen production and recovery by membrane gas separation. *Desalination.* 2009;240(1–3):306–310.
 46. Ardaneh M, Abolhasani M, Esmaeili M. CFD modeling of two-stage H₂ recovery process from ammonia purge stream by industrial hollow fiber membrane modules. *Int J Hydrogen Energy.* 2019;44(10):4851–4867.
 47. Farjami M, Moghadassi A, Vatanpour V. Modeling and simulation of CO₂ removal in a polyvinylidene fluoride hollow fiber membrane contactor with computational fluid dynamics. *Chem Eng Process Process Intensif.* 2015;98:41–51.
 48. Shirazian S, Moghadassi A, Moradi S. Numerical simulation of mass transfer in gas-liquid hollow fiber membrane contactors for laminar flow conditions. *Simul Model Pract Theory.* 2009;17(4):708–718.
 49. Oxarango L, Schmitz P, Quintard M. Laminar flow in channels with wall suction or injection: a new model to study multi-channel filtration systems. *Chem Eng Sci.* 2004;59(5):1039–1051.
 50. Sellars JR. Laminar flow in channels with porous walls at high suction reynolds numbers. *J Appl Phys.* 1955;26(4):489–490.
 51. Berman AS. Laminar flow in channels with porous walls. *J Appl Phys.* 1953;24(9):1232–1235.

52. Scholes CA, Simioni M, Qader A, Stevens GW, Kentish SE. Membrane gas-solvent contactor trials of CO₂ absorption from syngas. *Chem Eng J*. 2012;195:188-197.
53. Günther J, Schmitz P, Albasi C, Lafforgue C. A numerical approach to study the impact of packing density on fluid flow distribution in hollow fiber module. *J Membr Sci*. 2010;348(1-2):277-286.
54. Asimakopoulou A, Karabelas A. Mass transfer in liquid-liquid membrane-based extraction at small fiber packing fractions. *J Membr Sci*. 2006;271(1-2):151-162.
55. Razavi SMR, Shirazian S, Nazemian M. Numerical simulation of CO₂ separation from gas mixtures in membrane modules: effect of chemical absorbent. *Arab J Chem*. 2016;9(1):62-71.
56. Ebadi Amooghin A, Sanaeepur H, Kargari A, Moghadassi A. Direct determination of concentration-dependent diffusion coefficient in polymeric membranes based on the Frisch method. *Sep Purif Technol*. 2011;82:102-113.
57. Ebadi Amooghin A, Moftakhari Sharifzadeh MM, Zamani Pedram M. Rigorous modeling of gas permeation behavior in facilitated transport membranes (FTMs); evaluation of carrier saturation effects and double-reaction mechanism. *Greenhouse Gases Sci Technol*. 2018;8(3):429-443.
58. Sanaeepur H, Ebadi Amooghin A, Khademian E, Kargari A, Omidkhah M. Gas permeation modeling of mixed matrix membranes: adsorption isotherms and permeability models. *Polym Compos*. 2018;39(12):4560-4568.
59. Ebadi Amooghin A, Jafari S, Sanaeepur H, Kargari A. Computational fluid dynamics simulation of bubble coalescence and breakup in an internal airlift reactor: Analysis of effects of a draft tube on hydrodynamics and mass transfer. *App Math Model*. 2015;39(5-6):1616-1642.
60. Hekmat A, Ebadi Amooghin A, Moraveji MK. CFD simulation of gas-liquid flow behaviour in an air-lift reactor: determination of the optimum distance of the draft tube. *Simul Model Pract Theory*. 2010;18(7):927-945.
61. Bagheripour E, Moghadassi A, Hosseini SM, Van der Bruggen B, Parvizian F. Novel composite graphene oxide/chitosan nanoplates incorporated into PES based nanofiltration membrane: chromium removal and antifouling enhancement. *J Ind Eng Chem*. 2018;62:311-320.
62. Gao J, Sun S-P, Zhu W-P, Chung T-S. Polyethyleneimine (PEI) cross-linked P84 nanofiltration (NF) hollow fiber membranes for Pb²⁺ removal. *J Membr Sci*. 2014;452:300-310.

How to cite this article: Maarefian M, Bandehali S, Azami S, Sanaeepur H, Moghadassi A. Hydrogen recovery from ammonia purge gas by a membrane separator: A simulation study. *Int J Energy Res*. 2019. <https://doi.org/10.1002/er.4819>

